Dalton Transactions

Nano-Gate Opening Pressures for the Adsorption of Isobutane, n-Butane, Propane, and Propylene Gases on bimetallic Co-Zn Based Zeolitic Imidazolate Frameworks

Journal:	*Dalton Transactions*
Manuscript ID	DT-ART-01-2019-000222.R2
Article Type:	Paper
Date Submitted by the Author:	07-Feb-2019
Complete List of Authors:	Awadallah-F , Ahmed; Qatar University, Dept of Chemical Engineering Hillman, Febrian ; Texas A&M University College Station, Chemical Engineering Al-Muhtaseb, Shaheen; Qatar University, Dept of Chemical Engineering Jeong, Hae-Kwon; Texas A

Nano-Gate Opening Pressures for the Adsorption of Isobutane, n-Butane, Propane, and Propylene Gases on bimetallic Co-Zn Based Zeolitic Imidazolate Frameworks

Ahmed Awadallah-F [(a),1], Febrian Hillman[(b)], Shaheen A. Al-Muhtaseb [(a),*] and Hae-Kwon Jeong [(b), (c)]

(a) Department of Chemical Engineering, Qatar University, P.O. Box 2713, Doha, Qatar

(b) Artie McFerrin Department of Chemical Engineering and (c) Department of Materials Science and Engineering, Texas A&M University, College Station, TX 77843-3122, United States

Abstract

In this article, a zeolitic-imidazolate framework-8 (ZIF-8) and its mixed metal CoZn-ZIF-8 were synthesized via a rapid microwave method. The products were characterized by Raman spectra, XPS, XRD, EDX, TEM, NanoSEM, TGA, and DSC. The gas adsorption properties of samples were carried out using C_3 and C_4 hydrocarbons, including propane, propylene, isobutane and n-butane at a temperature of 25 °C. The adsorption equilibrium and kinetics of these gases on various ZIFs were studied. It was noticed that ZIF-8 and mixed metal CoZn-ZIF-8 samples start to adsorb these gases after certain pressures which are believed to result in opening their nano-gates (i.e., 6 membered rings) to allow the entry of the gas molecules. The nanogate opening pressure value (p_0) for each ZIF towards different gases was determined by fitting adsorption equilibrium data against a modified form of the Langmuir adsorption isotherm model. It was observed that the value of p_0 differs significantly for each gas, and with various extents for various ZIFs. Therefore, it is possible that the distinct values of p_0 afford a unique technique to separate and purify these gases at industrial scale. The overall mass transfer coefficient values of adsorption process were also investigated.

***Keywords**: Mixed metal CoZn-ZIF-8; nanogate opening pressure; Adsorption equilibrium; Adsorption kinetics; Fast microwaves technique*

**Corresponding Author. Tel.(+974) 4403-4139; Fax: (+974) 4403-4131; E-mail: s.almuhtaseb@qu.edu.qa*

[1] On leave from the Radiation Research of Polymer Department, National Centre for Radiation Research and Technology, Atomic Energy Authority, P.O. Box 29, Nasr City, Cairo, Egypt

Introduction

Metal–organic frameworks (MOFs) are porous crystalline materials forming from metal ions or metal-containing clusters coordinated to rigid organic molecules to form geometrical dimensions of networks. MOFs have made a spotlight on their importance and their unique features (such their highly porosity, huge surface areas, low density, and the chemical tenability of their structures).[1-4] Zeolitic-imidazolate frameworks (ZIFs) are among the most promising members of the MOFs family. This is due to their high porosity, relative stability, and ease of preparation. Therefore, ZIFs are ideal candidates for various applications such gas storage,[5] gas separation,[6,7] catalysis[8] and drug delivery.[9] ZIFs are formed from tetrahedral units, in which each metal ion (typically Zn^{2+} or Co^{2+}) connects four imidazolate-based ligands to form three-dimensional porous frameworks.[10,11] ZIF-8 ($Zn(mIm)_2$, where mIm = 2-methylimidazolate), with the sodalite (SOD) topology, crystallizes in the cubic space group $I\bar{4}3m$ with a lattice constant of 16.992 Å and contains 276 atoms in the unit cell ($Zn_{12}N_{48}C_{96}H_{120}$).[12] The sodalite cages possess a cavity diameter of 11.6 Å, and a defined aperture of 3.4 Å.[13] ZIF-8 is known unusually for its high thermal and chemical stability.[14] Recently, many researchers have utilized the synthetic flexibility offered by ZIFs (more generally MOFs) to obtain novel structures, thereby functionalities.[15-17] One such approach is by introducing mixed metal centers and/or linkers in their frameworks, resulting in hybrid materials with tunable porosity and surface properties.[1, 6] Jeong's group[2, 3] and others[4-7] have exposed that mixing metal centers and linkers can tune the framework molecular sieving properties (including gas diffusivity, linker flip-flopping motion, etc.), hydrophobicity and polarity. For example, substituting Zn ions in ZIF-8 framework with Co ions can increase the "stiffness" in the metal—nitrogen (M—N) bonding[3, 8] reducing its effective aperture size.[9] As a result, the Co substituted ZIF-8 (formerly known as ZIF-67) enhanced the separation selectivity for propylene and propane binary mixture.[3,8] Linker exchange on the 2-methylimidazole (mIm) of ZIF-8 with less bulky imidazole-2-carboxaldehyde can enhance the diffusivity of butanes isomer.[6] On the other hand, substituting mIm with bulky benzimidazole linker can decrease the framework effective aperture, enhancing its separation selectivity on different gas mixtures.[2]

It was reported from literature recently that Zn^{2+} ions in the ZIF-8 lattice can be replaced by the Co^{2+} ions, which imparts products with new features.[18,19] The various techniques for the synthesis of bimetallic Zn/Co-ZIF-8 have been previously mentioned in the literature.[20,21] Kaur et al[20]

mentioned that the bimetallic Zn/Co-ZIF-8 can increase the pore volume and active surface area in compared to ZIF-8 sample. Further, Wang et al[22] reported that it could be synthesized the Zn/Co-ZIF-8 membranes for separation of gas mixture. Through results, it was found that the selectivity of the membranes to one of these gases decreases with increasing the Co^{2+}/Zn^{2+} ratio in the bimetallic ZIF matrix. It was demonstrated that mixing of ZIF-8 by Co^{2+} improves the photodegradation of methylene blue dye using a UV irradiation without H_2O_2.[23]

Li et al[24] investigated the effect of single-component diffusion rates on the kinetic separation of propane/propene gases by a series of metal imidazolate zeolitic framework materials, and they concluded that the separation depended highly on the significant differences between their diffusion rates into the pore systems. Further, Li et al[24] reported from various references[25] that "for a few eight-membered ring zeolites, separation of light hydrocarbons such as propane and propene is controlled by the critically sized pore openings". Zhang et al[26] investigated the molecular sieving features of ZIF-8 by evaluating the thermodynamically corrected diffusivities of *iso*-C_4H_8/*iso*-C_4H_{10} and *n*-C4H_{10}/*iso*-C_4H_{10} at a given temperature and found an interesting and unexpected behavior that "because of aperture flexibility", the studied C4 hydrocarbon molecules that are larger than the effective aperture size still adsorb in the micropores of ZIF-8.

Microwave-assisted preparation has recently become popular in MOF synthesis as a facile, rapid, inexpensive, and commercially viable route toward the production of these crystalline substances.[19,27-31] Recently, Hillman et al[2] successfully prepared multiple mixed linkers and/or metal ZIFs through a microwave-assisted technique, which significantly decreased the preparation time, improved the yield percentage, and decreased the crystal size distributions. Herein, we expose a rapid and facile synthesis of mixed metal CoZn-ZIF-8through a microwave-assisted approach, in which Zn/Co-ZIF-8 can be obtained in a period of 1.5 min. In the course of our studies related to the construction of ZIF-8 derived hybrid materials displaying adsorption affinities towards alkane gases, we sought to study the consequences of Co^{2+} mixing on the Zn-ZIF-8 framework.

This study utilizes the approach of fast microwave preparation to the ZIF-8 and its mixed metal CoZn-ZIF-8 (hereafter so called Zn/Co-ZIF-8) adsorbents for adsorption of propane, propylene, n-butane and isobutane. We report a phenomenon in which the adsorption behavior

depends on a threshold pressure that stimulates nano-gate opening (which is hereafter denoted as nanogate opening pressure, p_0) during adsorption on ZIF samples. The samples of ZIF-8 or its mixed metal Co/Zn-ZIF-8 are characterized by Raman spectra, XPS, XRD, EDX, TEM, NanoSEM, TGA and DSC. The gases utilized in the adsorption processes are propylene, propane, n-butane and isobutane. The p_0 values for the adsorption of propylene, propane, n-butane and isobutane gases onto different ZIF samples were examined at 25^{o}C. Furthermore, an investigation of the rate of adsorption was carried out in order to estimate the overall mass transfer coefficient value of each gas/adsorbent system.

Experimental

Materials

Zinc nitrate hexahydrate ($Zn(NO_3)_2.6H_2O$, 98%, Sigma Aldrich) and cobalt nitrate hexahydrate ($Co(NO_3)_2.6H_2O$, ≥ 98%, Sigma Aldrich) were used as metal sources. 2-Methylimidazole ($C_4H_5N_2$, 97%, Sigma Aldrich) was used as ligand sources. Methanol (99.8%, Alfa Aesar) was used as a solvent. Different gases used (i.e., n-butane, isobutane, propane and propylene) were of high purity (99.5%) and purchased from the National Industrial Gas Plants (NIGP, Qatar). All chemicals were used as purchased without further purification.

Microwave synthesis of mixed metal Zn/Co-ZIF-8

The synthesis of Zn-ZIF-8 using microwave-assisted approach is similar to previously reported by our group.[3] Briefly, 4.45 mmol of zinc nitrate hexahydrate ($Zn(NO_3)_2.6H_2O$) were dissolved in 15 mL of methanol and labeled as metal solution. The linker solution was prepared separately by dissolving 17.8 mmol of 2-methylimidazole in 15 mL of methanol. The metal solution was then poured into the linker solution while continuously stirring the solution for 1 min. The mixed solution was transferred to a microwave-transparent glass tube, followed by microwave irradiation with a power of 100 W for 1.5 min. The solution was then allowed to sit at ambient temperature to cool for 30 min. The precipitate was collected by centrifuging the cooled solution at 8000 RPM for 30 min. The resulting powder was washed in 30 mL of methanol three times, followed by drying in an oven at 120 °C for 12 hours prior to characterization. For the synthesis of Co-ZIF-8, the zinc nitrate hexahydrate is replaced with 4.45 mmol of cobalt nitrate hexahydrate in the metal

solution above. For the synthesis of Zn/Co-ZIF-8, the metal solution is replaced with mixture of 2.225 mmol of zinc nitrate hexahydrate and 2.225 mmol of cobalt nitrate hexahydrate dissolved in 15 mL of methanol.

Charaterziation

The FT-Raman spectra were measured by using a Bruker FT-Raman spectrometer of type RFS 100/S that is attached to a Bruker-IFS 66/S spectrometer, which provides high resolution to better than 0.10 cm^{-1}. Bruker's patented frictionless interferometer with its rock solid alignment that provides high sensitivity and stability. The diode-pumped, air-cooled Nd: YAG laser source with maximum laser power of 1500 mW at 1064 nm is controlled with full automation. The standard RFS 100/S configuration provides a spectral range of 70 –3600 cm^{-1} (Stokes shift) and 100 to 2000 cm^{-1} (anti-Stokes shift). The morphology of ZIFs was observed with a FEI Nova™ nanoscanning electron microscopy 450 (Nova NanoSEM). The chemical compositions of samples were investigated by Energy-dispersive X-ray spectroscopy (EDX) attached to Nova NanoSEM. Transmission electron microscopy of FEI Tecnai G2 F20. X-ray photoelectron spectroscopy (XPS) was performed using a Thermo Scientific K-alpha photoelectron spectrometer with monochromatic Al_{ka} radiation. X-ray diffraction (XRD) measurements were conducted by using Miniflex II Benchtop XRD apparatus, manufactured by Rigaku Corporation Japan. The 2θ scan data were collected at 0.05° intervals over the range of 5 to 90°, and at a scan speed of 0.05°/min. Thermogravimetric analyses (TGA) were carried out using a PerkinElmer Pyris6 TGA analyzer under an N_2 gas in the range of 30^{o}C to 800^{o}C with a heating rate of 10^{o}C/min. Differential scanning calorimetry (DSC), PerkinElmer, Jade DSC, was used with a temperature range from 25 to 450^{o}C. The adsorption equilbrium of isobutane, n-butane, propylene and propane gases were measured by a magnetic suspension microbalamce (MSB) (Hygra, Rubotherm) with a microgram sensitivity. The degassing process was done under vacuum (0.05 bar) at 107^{o}C for 3 days. More details on the experimental procedure and data analyses involved in measuring the adsorption equilibrium and kinetics are found elsewhere.[27, 28]

Results and discussion

Preparation and characterization

The mixed metal CoZn-ZIF-8 (termed Zn/Co-ZIF-8) has been successfully prepared rapidly via a microwave-assisted in-situ technique. Two cobalt mixed ZIF-8 samples were prepared with 50 and 100% Co, termed Zn/Co-ZIF-8 and Co-ZIF-8, respectively, and their properties are compared to pristine ZIF-8.

The NanoSEM morphology photomicrographs of ZIF-8, Zn/Co-ZIF-8 and Co-ZIF-8 declare that all crystals are in nanosized scale with relatively uniform size distributions as presented in **Figure 1 (a-d)**. Both the ZIF-8 and the mixed metal CoZn-ZIF-8 crystals possess SOD topology, agreeing with reported results in literature [12]. Overall, it was seen that by inserting the Co^{2+} metal ion into the reaction solution, the produced nanocrystal size increases (**Figure 1d**). Therefore, the sequential order of these samples are Zn/Co-ZIF-8 > Co-ZIF-8 > ZIF-8; with mean particle sizes of 127, 77 and 63 nm, respectively. The means, modes and standard deviations of particle size distributions are listed within Figure 1d. The nanosized crystals and the uniformity of the crystal size owe likely to the homogenous volumetric heating in combination with fast temperature increment during the exposure to the microwave irradiation.[3,14] **Figure 2** shows the TEM images of ZIF-8, Zn/Co-ZIF-8 and Co-ZIF-8 samples, respectively. Generally, it was observed that by insertion Co^{2+} in to solution media, the crystal sizes of formed product ZIFs are affected. There are other characterizations such XRD, Raman spectra, TGA&DSC, XPS and EDX were found as **Fig.S1, Fig.S2, Fig.S3, Fig. S4** and **Fig. S5** in ***Supplementary Data File,*** respectively.

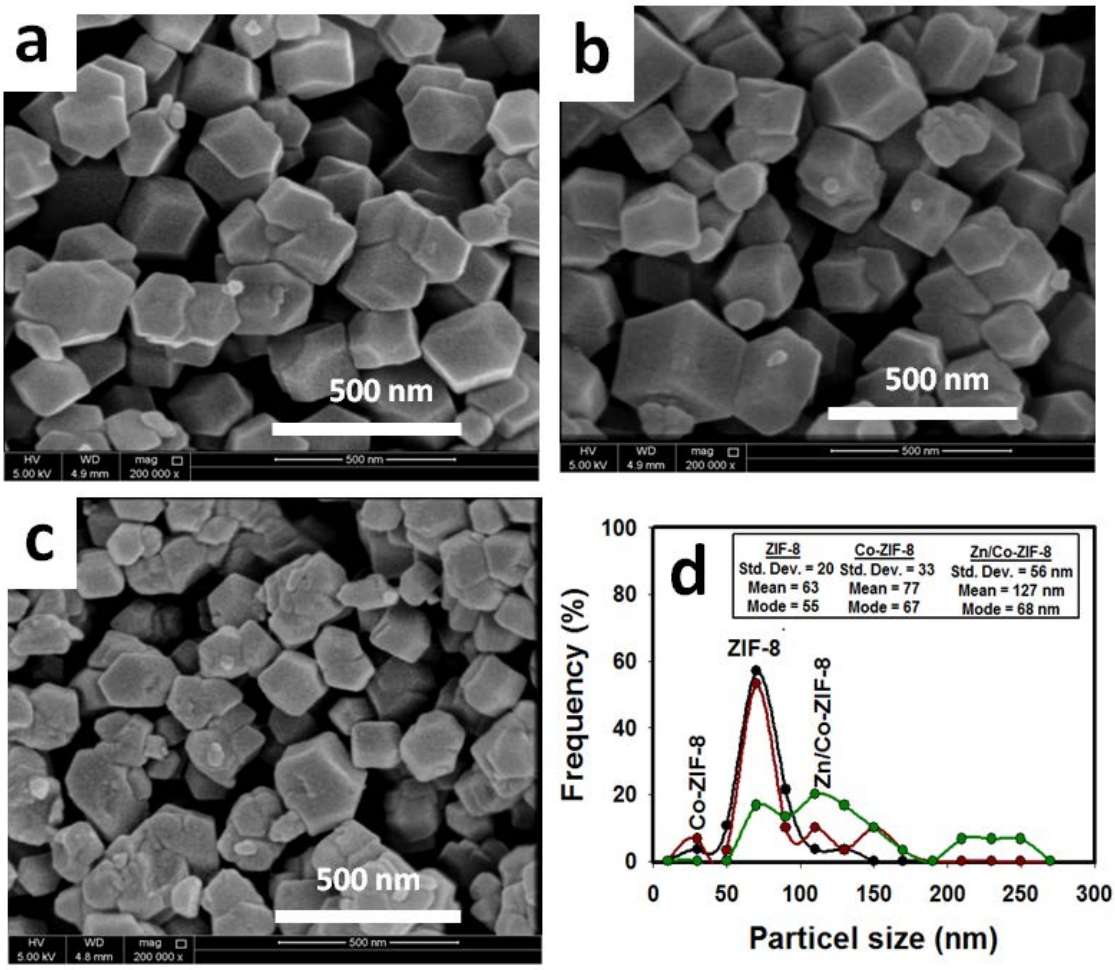

Figure 1. NanoSEM photomicrographs of (a) ZIF-8, (b) Zn/Co-ZIF-8 and (c) Co-ZIF-8. Subfigure (d) shows the particle size distributions of ZIF-8, Zn/Co-ZIF-8 and Co-ZIF-8 samples as obtained from SEM images.

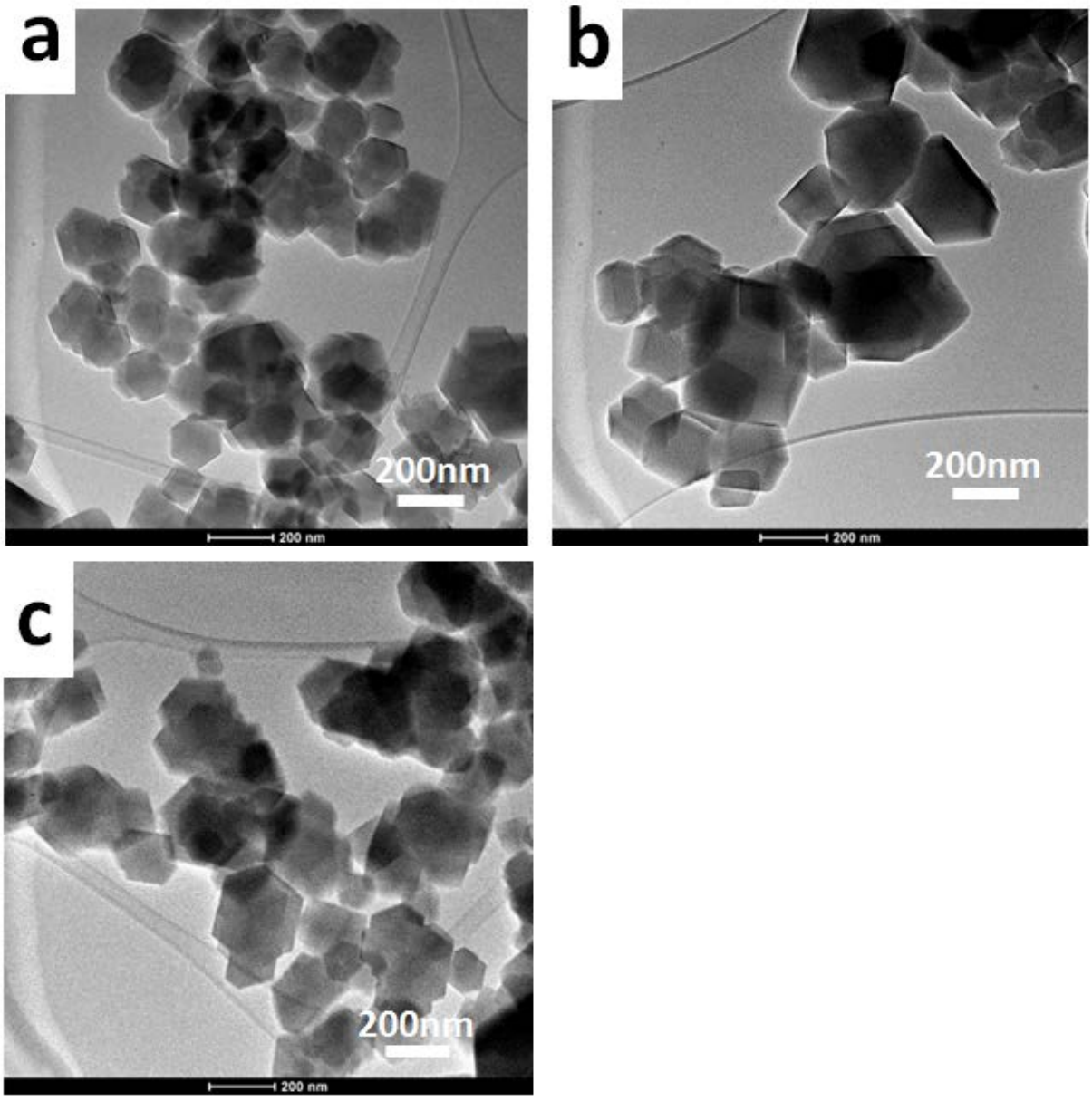

Figure 2. TEM images of different ZIF samples (a) ZIF-8, (b) Co-ZIF-8 and (c) Zn/Co-ZIF-8.

Table 1. Elemental analysis of various ZIFs by using XPS and EDX techniques.

Elements (atomic conc.%)	**XPS analysis**		
	ZIF-8	Zn/Co-ZIF-8	Co-ZIF-8
C 1s	64	66	63
N 1s	25	22	23
O 1s	1	4	4
Zn 2p	10	6	-
Co 2p	-	2	10
Elements (atomic conc.%)	**EDX analysis**		
	ZIF-8	Zn/Co-ZIF-8	Co-ZIF-8
C	66	68	66
N	14	22	26
O	2	3	3
Zn	18	4	-
Co	-	3	5

.

Adsorption equilibria

As shown in **Figures 3-5**, the tested ZIF-8, Co-ZIF-8 and Zn/Co-ZIF-8 samples illustrates a similar trend towards the adsorption of relatively long-chained hydrocarbon gases, where the samples remain irresponsive to the pressure increase up to a moderate pressure value, after which they expose a type-I adsorption isotherm. Therefore, authors in this study suggest a modified form of the Langmuir adsorption isotherm model as:

$$n = \frac{m\, b\, (p - p_0)}{1 + b\, (p - p_0)}, \quad p \geq p_0 \qquad (1)$$

where n refers to amount adsorbed (mole/kg), p to the exposure pressure, m to monolayer adsorption capacity, b to the adsorption affinity, and p_0 to the nanogate opening pressure. The p_0

value indicates a pressure threshold at which the ZIF crystal is believed to open (widen) its nanogate to allow the adsorption of a specific gas molecule. Before this point (i.e., $p < p_0$), the nanogate of the ZIF crystal is believed to be partially closed, which hinders the passage of the molecules into the crystal and thus exhibits nil adsorption.

It is noteworthy to mention that p_0 in Eq. (1) is a new parameter that was introduced into Langmuir model by authors. Eq. (1) represents a finite Henry's Law constant for the affinity of gas adsorption on a clean surface (when $[p - p_0] \rightarrow 0$) as seen in Eq. (2), which hints to its thermodynamic consistency when p is above p_0.

$$H' = \lim_{(p-p_0)\rightarrow 0} \left(\frac{n}{p-p_0}\right) = m\ b \qquad (2)$$

The gas adsorption of propane, isobutane and propylene onto the three samples; ZIF-8, Co-ZIF-8 and Zn/Co-ZIF-8 are exhibited in **Figs. (3-**5), respectively. Overall, it is noticed from the three figures that the equilibrium adsorption of all samples increase by increasing the pressure, but the adsorption of each gas starts to occur after a threshold pressure value, which is pre-defined previously by p_0. It is observed from **Fig.3a** that n-butane exposes the highest equilibrium adsorption capacity onto ZIF-8, whereas propylene represents the lowest equilibrium adsorption capacity. The order of equilibrium adsorption capacity of gases onto ZIF-8 is n-butane > propane > isobutane ≈ propylene. The Langmuir fitting parameters of these gases on various ZIFs, along with p_0 values are listed in **Table 2**.

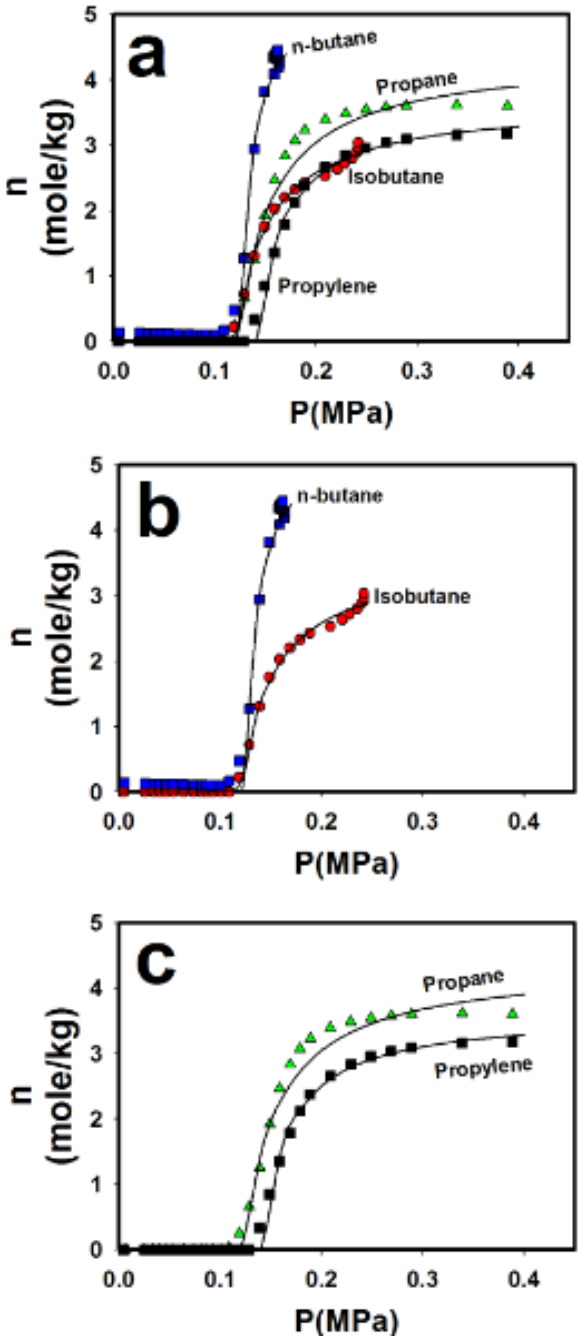

Figure 3. Equilibrium adsorption isotherms of n-butane, propane, isobutane and propylene gases onto ZIF-8 at 25°C. Symbols indicate to experimental points and solid lines indicate to the fitting of modified Langmuir model. Subfigure (a) shows a comparison of the isotherms of the four gases, whereas subfigure (b) shows a comparison between the isotherms of n-butane and isobutane gases, and subfigure (c) shows a comparison between the isotherms of propane and propylene gases.

Figure 3b describes how the equilibrium adsorption capacity of n-butane exceeds that of isobutane significantly. Considering that both n-butane and isobutane have the same chemical formula (C_4H_{10}) and molecular mass (58.12 g/mol), this difference may be assignable to the stereochemistry of each gas. The n-butane is a linear chain molecule, which can invade the nano-gate with less difficultly; whereas isobutane is a branched molecule, which causes it to confront a difficulty entering the nanogate of ZIF-8. However, the opening pressures (p_0) for the adsorption of n-butane and isobutane (i.e., the intermediate pressure at which the isotherm curve starts to appear) is almost equal. Therefore, there is a difficulty to separate n-butane and isobutane gases. This is due to the approaching values of p_0 for both gases, which are 0.126 and to 0.121 MPa for n-butane and isobutane gases, respectively. Nonetheless, ZIF-8 can be used to separate n-butane from isobutane based on difference in adsorption capacities at higher pressures.

It is seen from **Figure 3(c)** that propane and propylene gases exposes almost similar (parallel) trends of adsorption isotherms, but the adsorption of propylene occurs at a higher p_0 value than propane. This is believed to be mainly due to its double bond, hinders the propylene gas molecule to invade the nano-gate of ZIF-8 upon adsorption. However, there is some difficulty to separate propane and propylene gases at their values of p_0. This is due to small different in p_0 values, which are equal to 0.123 and 0.142 MPa for propane and propylene gases, respectively.

Figure 4a illustrates the equilibrium adsorption isotherms of n-butane, propane, isobutane and propylene gases onto Co-ZIF-8 at 25 °C. Generally, it can also be observed that the n-butane exhibits the highest equilibrium adsorption capacity and isobutane gas exhibits the lowest adsorption capacity onto Co-ZIF-8. The order of equilibrium adsorption capacities onto Co-ZIF-8 are n-butane > propylene > propane > isobutane. Further, it is observed that from **Fig.4b** that a small difference starts to appear between the p_0 values of n-butane and isobutane gases. Therefore, it could be deduced that the Co-ZIF-8 adsorbent can be utilized to separate these two gases at an intermediate pressure between their distinct p_0 values, which are equal to 0.132 and 0.109 MPa, for n-butane and isobutane, respectively. So, at an intermediate pressure (e.g., 0.120 MPa), only isobutane will be adsorbed (unlike n-butane). Similarly, **Figure 4c** indicates that it is also probable to a great extent to separate the propylene from propane gases based on the difference between

their p_0 values. The p_0 values of propylene gas and propane gas are 0.097 and 0.055 MPa, respectively. The fitting parameters of modified Langmuir are registered in **Table 2**.

Figure 5a exhibits the equilibrium adsorption isotherms of n-butane, isobutane, propylene and propane gases onto Zn/Co-ZIF-8. It was seen that the equilibrium adsorption capacity of n-butane is the highest value, while propane is the lowest value. The sequential order of equilibrium adsorption capacity onto Zn/Co-ZIF-8 at monolayer saturation is as n-butane > propylene > isobutane > propane. The modified Langmuir model fitting parameters are registered in **Table 2**. It was observed from **Figs 5b and 5c** that n-butane gas can be separated from isobutane gas, and propane gas can be separated from propylene gas based on their different p_0 values. For example, the p_0 values corresponding to n-butane and isobutane gases are 0.133 and 0.112 MPa, respectively; whereas the p_0 values for propane and propylene gases are to 0.123 and 0.115 MPa, respectively, as registered in **Table 2**. Therefore, it can be said from emerged results that the Co-ZIF-8 is more capable than Zn/Co-ZIF-8 and ZIF-8 adsorbents to separate gases of competitive separations on the basis of their p_0 values. **Figure S6** shows the variation of nanogate opening pressure (p_0) values of the adsorption of different gases at 25^{o}C onto ZIF-8, Co-ZIF-8 and Zn/Co-ZIF-8 samples (see ***Supplementary Data File***).

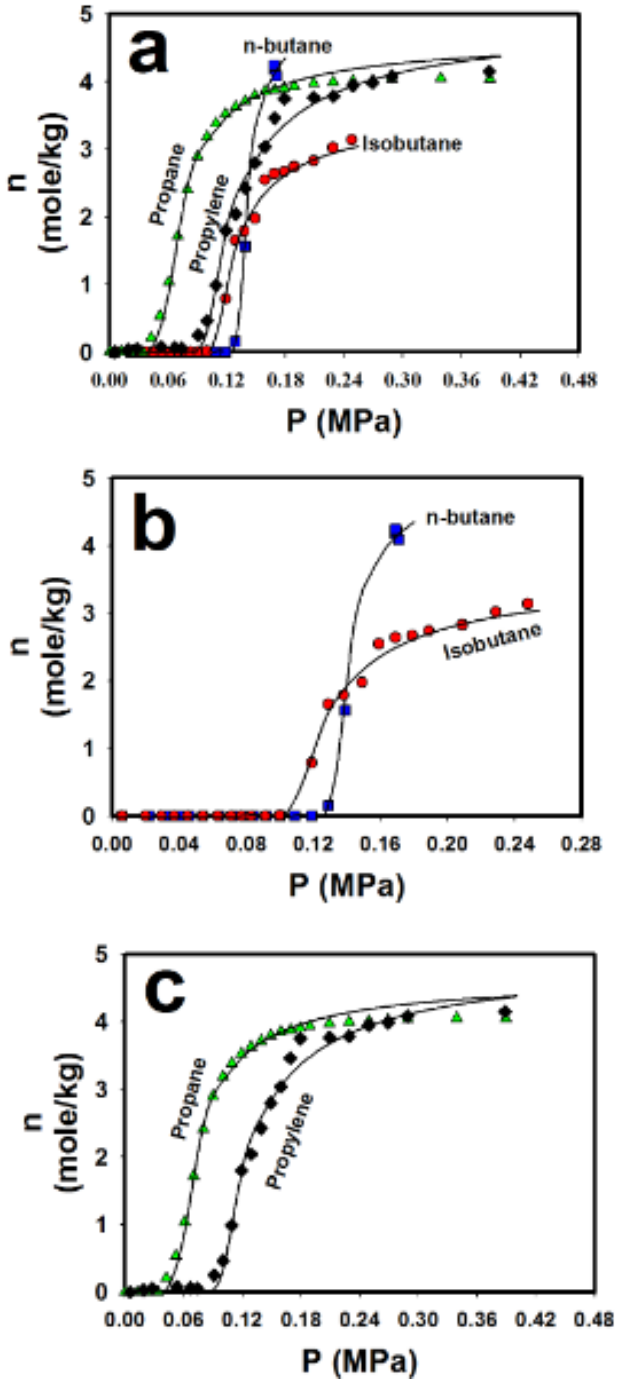

Figure 4. Equilibrium adsorption isotherms of n-butane, propane, isobutane and propylene gases onto Co-ZIF-8 at 25 °C. Symbols refer to experimental points and solid lines refer to fitting of modified Langmuir model. Subfigure (a) shows a comparison of the isotherms of the four gases, whereas subfigure (b) shows a comparison between the isotherms of n-butane and isobutane, and subfigure (c) shows a comparison between the isotherms of propane and propylene.

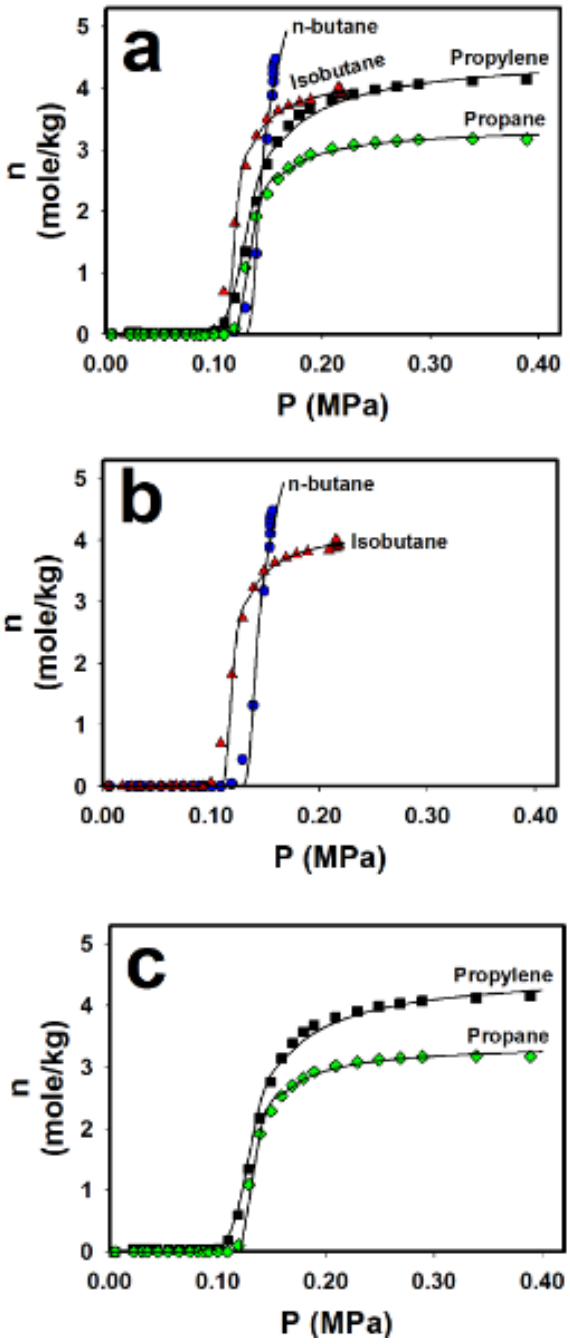

Figure 5. Equilibrium adsorption isotherms of n-butane, propane, isobutane and propylene gases onto Zn/Co-ZIF-8 at 25 °C. Symbols refer to experimental points and solid lines refer to fitting of modified Langmuir model. Subfigure (a) a comparison of the isotherms of the four gases, whereas subfigure (b) shows a comparison between the isotherms of n-butane and isobutane, and subfigure (c) shows a comparison between the isotherms of propane and propylene.

Table 2. Fitting parameters for the adsorption of different gases onto various ZIFs at 25°C.

ZIFs	Parameter	Gas			
		Propane	Propylene	Isobutane	n-butane
ZIF-8	*m (mole/kg)*	4.373	3.611	3.621	5.485
	b (MPa^{-1})	29.955	38.769	31.278	90.395
	p_o (MPa)	0.123	0.142	0.121	0.126
	LSSE	0.061	0.148	0.130	0.421
	ARE (%)	6.30	1.70	2.20	1.10
Zn/Co-ZIF-8	*m (mole/kg)*	3.383	4.555	4.264	8.074
	b (MPa^{-1})	86.466	48.191	118.071	47.554
	p_o (MPa)	0.123	0.115	0.112	0.133
	LSSE	0.02	0.364	0.511	0.431
	ARE (%)	1.0	7.8	0.9	6.5
Co-ZIF-8	*m (mole/kg)*	4.661	4.917	3.587	5.249
	b (MPa^{-1})	45.518	26.472	38.472	102.472
	p_o (MPa)	0.055	0.097	0.109	0.132
	LSSE	0.384	0.459	0.151	0.244
	ARE (%)	2.4	6.4	6.1	8.3

Figure 6 (a-d) shows the influence of ZIF-8, Zn/Co-ZIF-8 and Co-ZIF-8 samples on the equilibrium adsorption isotherms of propane, propylene, isobutene and n-butane gases at 25 °C. On the overview of **Fig.6a**, it is noticed that by increasing the pressure beyond the threshold of p_0, the equilibrium adsorption capacity of propane gas increases. Furthermore, by increasing the content of cobalt into the ZIF composition, the equilibrium adsorption capacity of the adsorbent increases in the range of p < ~ 0.2 MPa. Afterwards, the adsorption of propane on ZIF-8, Zn/Co-ZIF-8 and Co-ZIF-8 reached saturation. At ~ 0.21 MPa, the adsorption capacity of ZIF-8 adsorbent reached monolayer saturation, which exhibits a higher adsorption capacity than that on Zn/Co-

ZIF-8. After the value of ~ 0.2 MPa, the adsorption capacity of ZIF-8 adsorption starts to exceed that on Zn/Co-ZIF-8. Further, the p_0 of adsorption on the three ZIFs occurred at the values of 0.12, 0.12 and 0.05 MPa for the adsorption of propane onto ZIF-8, Zn/Co-ZIF-8 and Co-ZIF-8 samples, respectively.

Figure 6b shows the adsorption of propylene gas onto ZIF-8, Zn/Co-ZIF-8 and Co-ZIF-8 samples. It is noticed that by increasing the cobalt content into the ZIF matrix, the adsorption capacity rises up to a pressure of ~ 0.14 MPa where the order of adsorption capacity of ZIFs is Co-ZIF-8 > Zn/Co-ZIF-8 > ZIF-8. After this pressure (i.e., at $p >$ 0.14 MPa), the ZIFs approach their saturation limits where Co-ZIF8 and Zn/Co-ZIF-8 become almost identical. Hence, the order of the adsorption capacity of propylene at equilibrium is as Co-ZIF-8 ≈ Zn/Co-ZIF-8 > ZIF-8. Further, the adsorption of propylene gas starts on ZIF-8, Zn/Co-ZIF-8 and Co-ZIF-8 are at the p_0 values of 0.14, 0.11 and 0.097 MPa, respectively.

It is observed from **Figure 6c** that by increasing the cobalt concentration into the ZIF matrix, the equilibrium adsorption capacity of n-butane gas decreases. The order of the equilibrium adsorption capacity is as ZIF-8 > Co-ZIF-8 ≈ Zn/Co-ZIF-8. Furthermore, the adsorption of n-butane starts at the p_0 values of ~0.13, 0.13 and 0.13 MPa for ZIF-8, Zn/Co-ZIF-8 and Co-ZIF-8 and, respectively.

Figure 6d represents the adsorption of isobutane gas onto ZIF-8, Zn/Co-ZIF-8 and Co-ZIF-8. Overall, it is seen that by increasing the cobalt content into the ZIF matrix, the adsorption capacity of ZIF towards isobutane increases up to 0.1 MPa where the order of adsorption capacities is Co-ZIF-8 > Zn/Co-ZIF-8 > ZIF-8. After that pressure, the adsorption capacity of Zn/Co-ZIF-8 sample became higher than that of Co-ZIF-8 where the order becomes Zn/Co-ZIF-8 > Co-ZIF-8 > ZIF-8.

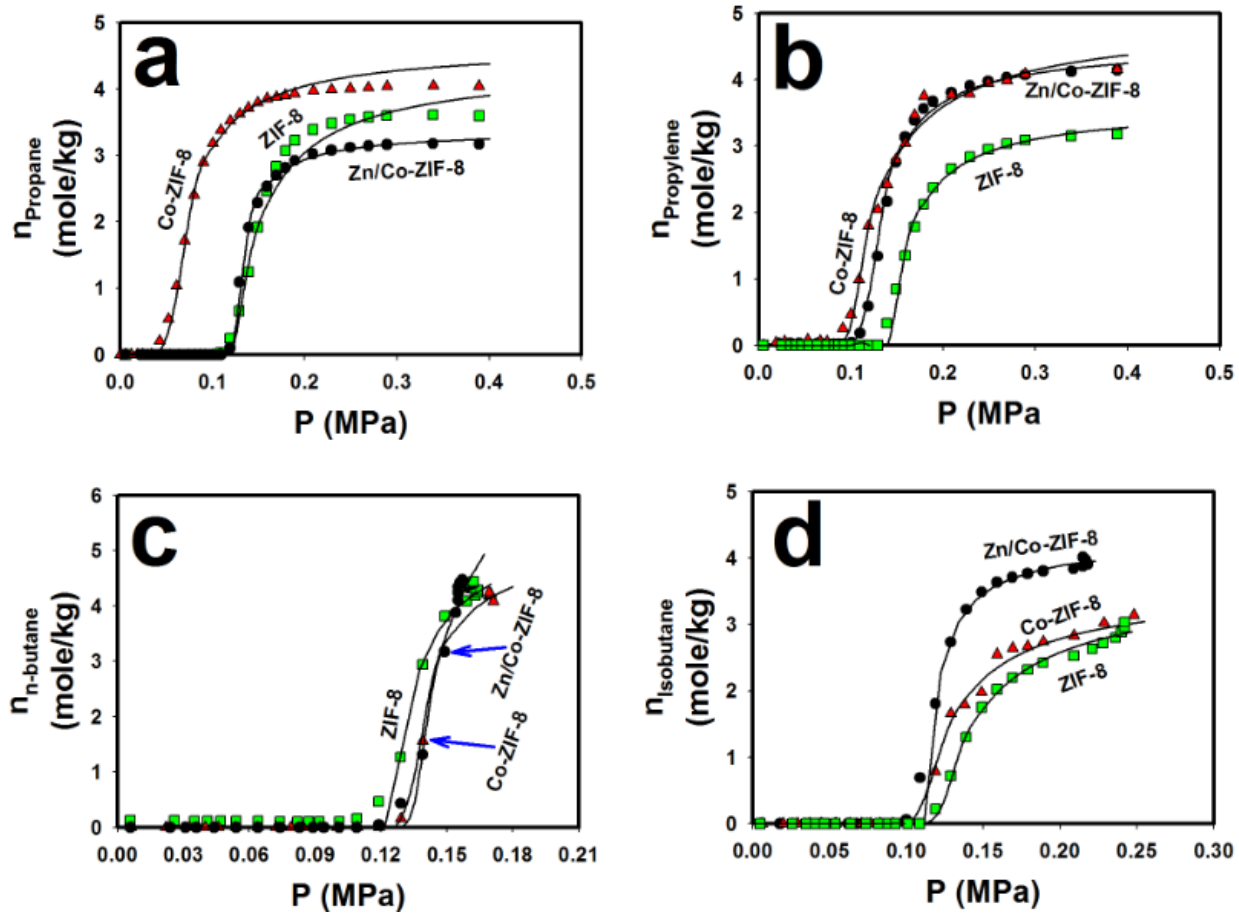

Figure 6. Effect of cobalt mixing ratio into ZIF-8 on the equilibrium adsorption capacity of (a) propane, (b) propylene, (c) n-butane and (d) isobutane at 25 °C. Symbols refer to experimental points and solid lines refer to the modified Langmuir model.

Rate of adsorption

The rate of adsorption can be determined by the linear driving force model,[16] which gives

$$\frac{m_t}{m_e} = 1 - e^{-kt} \qquad (3)$$

where m_t indicates the amount adsorbed at time t, m_e is the equilibrium amount adsorbed at the a certain temperature and pressure; and k is the overall mass transfer coefficient.

Figure 7 (a-d) shows the relationship between the overall mass transfer coefficient (k) for the adsorption of propane, propylene, n-butane and isobutane gases onto ZIF-8, Zn/Co-ZIF-8 and Co-ZIF-8 and versus reciprocal of pressure 1/P (MPa^{-1}) at 25 °C. It was noticed that by decreasing the parameter 1/P (i.e., increasing pressure), the overall mass transfer coefficient decreases for all samples. Further, as a noticeable behavior, the presence of cobalt into the ZIF structure has a significant impact on the k value for all ZIFs. Therefore, it could be deduced that the rate of adsorption affects by presence of cobalt ions into ZIFs. The order of the overall mass transfer coefficient for the adsorption of propane, propylene, n-butane and isobutane gases onto ZIFs is Zn/Co-ZIF-8 > Co-ZIF-8 > ZIF-8.

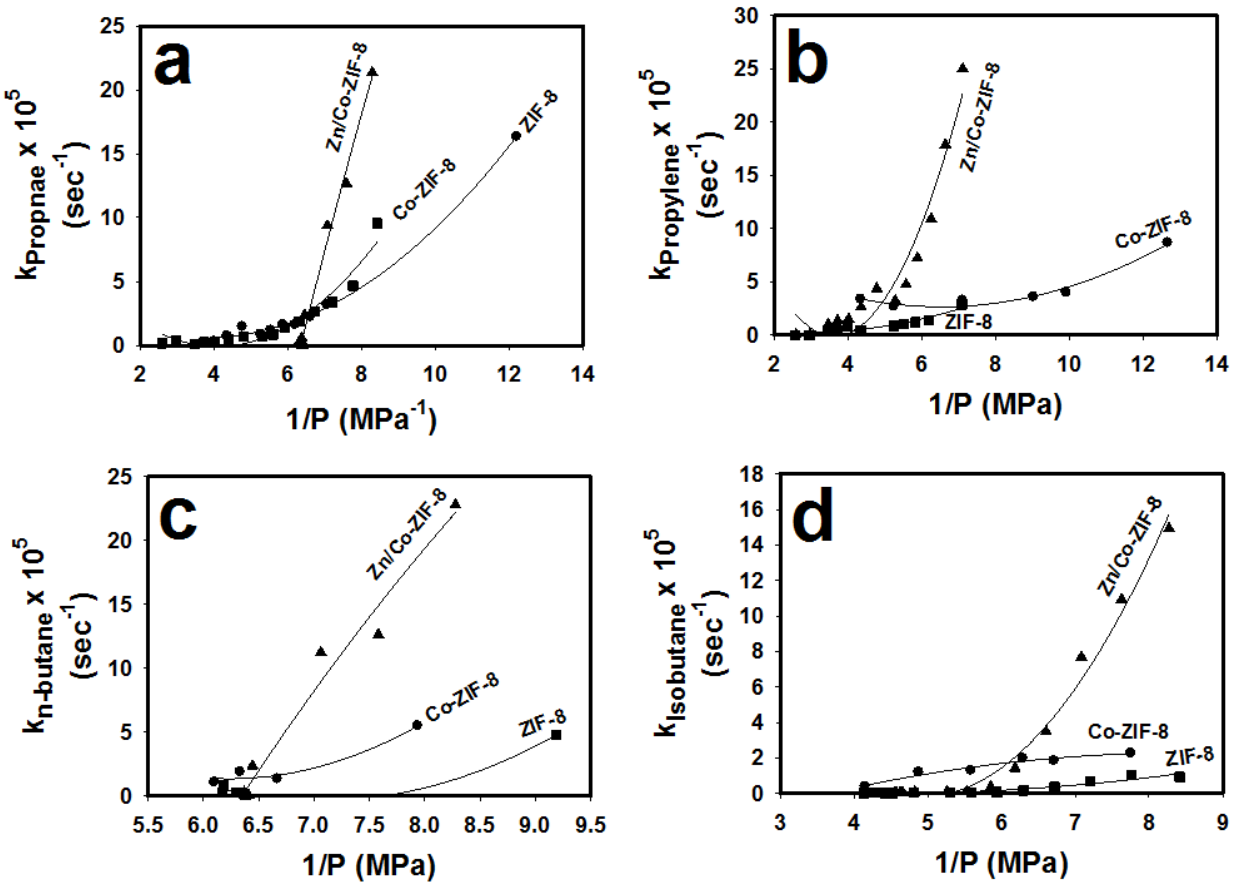

Figure 7. Overall mass transfer coefficient (*k*) deduced form first order kinetic versus 1/P for the adsorption of (a) propane, (b) propylene, (c) n-butane and (d) isobutane on ZIF-8, Zn/Co-ZIF-8 and Co-ZIF-8 at 25 °C.

Figure 8 (a-c) shows the relationship between overall mass transfer coefficient (*k*) and the reciprocal of exposed pressure (1/P) onto ZIF-8, Zn/Co-ZIF-8 and Co-ZIF-8 samples. Overall, it is observed from **Fig. 8a** that on ZIF-8, the adsorption of propane gas is the fastest, whereas the adsorption of isobutane is the slowest. On the other hand**.** It could be deduced from **Fig. 8b** that the highest rate of adsorption on Zn/Co-ZIF-8 is for propylene gas, while the slowest adsorption is of isobutane. Therefore, it can be seen that the kinetics of adsorption for various gases depends on the composition of the used ZIF. Furthermore, **Fig. 8c** shows that isobutane exhibits the highest rate of adsorption on Co-ZIF-8 whereas the slowest was n-butane.

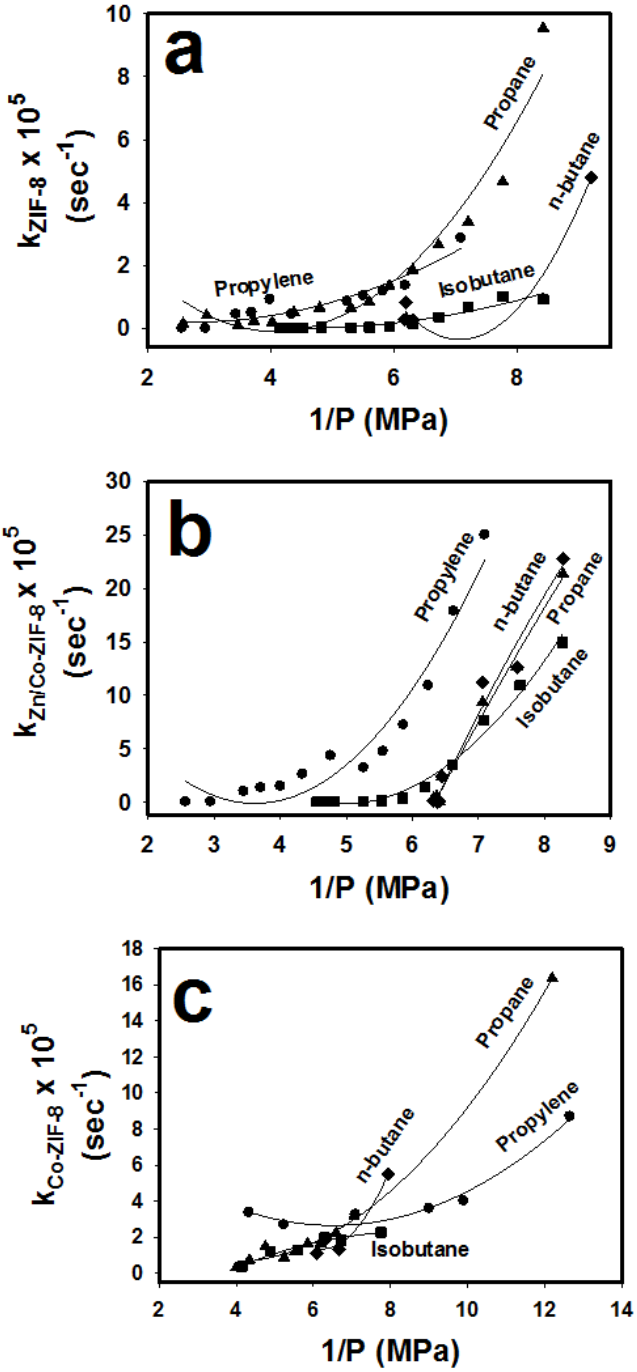

Figure 8. Overall mass transfer coefficient (k) deduced form first order kinetic versus 1/P for the adsorption of different gases onto (a) ZIF-8, (b) Zn/Co-ZIF-8 and (c) Co-ZIF-8 at 25 °C.

Conclusions

Three samples of ZIF family were prepared by zinc nitrate hexahydrate and cobalt nitrate hemi (pentahydrate) using a novel fast microwave technique. These samples are ZIF-8, Zn/Co-ZIF-8 and Co-ZIF-8. The prepared samples were characterized by Raman spectra, XPS, XRD, EDX, NanoSEM, TGA and particle size distributions. These ZIF-8 samples were utilized in the adsorption of isobutane, n-butane, propane and propylene gases at 25 °C, where the adsorption equilibrium and kinetics were investigated. The novel concept of having a threshold pressure (p_0) for the nano-gate opening of ZIFs for the adsorption of such gases was analyzed and discussed. It is to be noted that this is only one possible hypothesis, whereas other hypotheses may prove to be viable upon further studies. Therefore, this mechanism still needs deeper investigations to be better understood. The outcome results showed that the value of p_0 variates for different gases, especially when a high cobalt content is introduced in the matrix of ZIF-8 sample. These differences of p_0 values may introduce a unique approach to separate and purify gases at intermediate pressures between their characteristic p_0 values. The differences among the adsorption capacities of propylene, propane, isobutane and n-butane gases onto different ZIFs were also studied. The values of the overall mass transfer coefficients for the adsorption of various gases on the different ZIFs were also investigated. Generally, the rate of adsorption and the adsorption capacities of different gases were affected with the cobalt content into the ZIF-8 matrix.

Conflicts of interest

There are no conflicts of interest to declare

Acknowledgements

This publication was made possible by the NPRP awards (NPRP 08-014-2-003 and NPRP-8-001-2-001) from the Qatar National Research Fund (a member of The Qatar Foundation). H.K.-J. acknowledges support from the National Science Foundation (CMMI-1561897). The statements made herein are solely the responsibility of the authors. Technical support from the Department of Chemical Engineering, the Central Laboratory Unit (CLU) and the Gas Processing Centre (GPC) at Qatar University is also acknowledged.

References

1 A. Dhakshinamoorthy, A. M. Asiric, H.Garcia, *Catal. Sci. Technol.*, 2016, **6,** 5238-5261.

2 F. Hillman, J. Brito, H.-K. Jeong, *ACS Appl. Mater. Interfaces*, 2018, **10,** 5586-5593.

3 F. Hillman, J. M. Zimmerman, S.-M. Paek, M. R. A. Hamid, W. T. Limd, H.-K. Jeong, *J. Mater. Chem. A*, 2017, **5,** 6090-6099.

4 J. Y. Hong, Y. Jung, D.-W. Park, S. Chung, S. Kim, *Electrochim. Acta*, 2018, **259,** 1021-1029.

5 I. Cota, F. F. Martinez, *Coord. Chem. Rev.*, 2017, **351,**189-204.

6 J. Wei, W. Neng-Xu, L. Ze-Rui, J.-R. Wang, X. Xu, C.-S. Chen, *Ceram. Int.*, 2016, **42,** 8949-8954.

7 Y. Wen, J. Zhang, Q. Xu, X.-T. Wu, Q.-L. Zhu, *Coord. Chem. Rev.*, 2018, **376,** 248-276.

8 H. T. Kwon, H.-K. Jeong, A. S. Lee, H. S. An, J. S. Lee, *J. Am. Chem. Soc.*, 2015, **137,**12304-12311.

9 Y. Wu, H. Chen, D. Liu, Y. Qian, H. Xi, *Chem. Eng. Sci.*, **2015,** 124, 144.

10 J. M. Schoenmakers, Post-synthesis modification of zeolitic imidazolate framework-8 (ZIF-8) via cation exchange, Utrecht University Repository, 2016. https://dspace.library.uu.nl/handle/1874/334148

11 K. Zhou, B. Mousavi, Z. Luo, S. Phatanasri, S. Chaemchuen, F. Verpoort, *J. Mater. Chem. A*, 2017,**5**, 952-957.

12 H. Wang, M. Jian, Z. Qi, Y. Li, R. Lui, J. Qu, X. Zhang, *Micropor. Mesopor. Mater.*, 2018, **259,** 171-177.

13 A. Schejn, A. Aboulaich, L. Balan, V. Falk, J. Lalevée, G. Medjahdi, L. Aranda, K. Mozeta, R. Schneider, *Catal. Sci. Technol.*, 2015, **5,** 1829-1839**.**

.

14 J. Zhang, X. Yan, X. Hu, R. Feng, M. Zhou, *Chem. Eng. J.*, 2018, **347,** 640-647.

15 B. Reif, C. Paula, F. Fabisch, M. Hartmann, M. Kaspereit, W. Schwieger, *Microp. Mesopor. Mater.*, 2019, **275,** 102-110.

16 M. Fan, F. Gaia, Y. Cao, Z. Zhao, Y. Ao, Y. Liu, Q. Huo, *J. Solid State Chem.*, 2019, **269,** 507-512**.**

17 J. Peng, H. Zhang, Y. Yan, *J. Solid State Chem.*, 2019, **269,** 203-211**.**

18 V. V. Butova, V. A. Polyakov, A. P. Budnyk, A. M. Aboraia, E. A. Bulanova, A. A. Guda, E. A. Reshetnikova, Y. S. Podkovyrina, C. Lamberti, A. V. Soldatov, *Polyhedron,* 2018, **154,** 457–464.

19 J. Yang , F. Zhang , H. Lu , X. Hong, H. Jiang, Y. Wu, L. Yadong, *Angew.Chem.Int.Ed.*, 2015,**54**,10889–10893.

20 G. Kaur, R. K. Rai, D. Tyagi, X. Yao, P. Z. Li, X. C. Yang, Y. L. Zhao, Q. Xu, S. K. Singh, *J. Mater. Chem. A*, 2016, **4,**14932-14938.

21 Z. Hu, Z. Y. Guo, Z. P. Zhang, M. L. Dou, F.Wang, *A.C.S. Appl, Mater. Interfaces*, 2018, **10,**12651-12658.

22 C. Q. Wang, F. Q. Yang, L. Q. Sheng, J. Yu, K. X. Yao, L. X. Zhang, Y. C. Pan, *Chem. Commun.***, 2016,** 52, 12578- 12581.

23 D. Saliba, M. Ammar, M. Rammal, M. Al-Ghoul, N. Hmadeh, *J. Am. Chem. Soc.*, 2018, **140,** 1812- 1823.

24 K. Li, D. H. Olson, J. Seidel, T. J. Emge, H. Gong, H. Zeng, J. Li, *J. Am. Chem. Soc*. 2009, **131,** 10368–10369.

25 D. M. Ruthven, S. Reyes, *Microporous Mesoporous Mater.* 2007, **104,** 59– 66. N. Hedin, G. J. DeMartin, W. J. Roth, K. G. Strohmaier, S. C. Reyes, *Miroporous Mesoporous Mater.* 2008, **109,** 327–334. J. Gason, W. Blom, A. van Miltenburg, A. Ferreira, R. Berger, F. Kapteijn, *Microporous Mesoporous Mater.* 2008, **115,** 585–593. P. A. Barrett, T. Boix, M. Puche, D. H. Olson, E. Jordan, H. Koller, M. A. Camblor, *Chem. Commun.* 2003, **17,** 2114–2115. D. H. Olson, M. A. Camblor, L. A. Villaescusa, G. H. Kuehl, *Microporous Mesoporous Mater.* 2004, 67, 27–33. J. H. ter Horst, S. T. Bromley, G. M. van Rosmalen, J. C. Jansen, *Microporous Mesoporous Mater.* 2002, **53,** 45–57.

26 C. Zhang, R. P. Lively, K. Zhang, J. R. Johnson, O. Karvan, W. J. Koros, *J. Phys. Chem. Lett.* 2012, **3**, 2130–2134.

27 X. Wu, W. Liu, H. Wu, X. Zong, Z. Jiang, *J. Membrane Sci.*, 2018, **548,** 309-318.

28 N. Chen, D. Chen, F. Wei, S. Zhao, Y. Luo, *Chem. Phys. Lett.*, 2018, **705,** 23-30.

29 Q. Li, W. Yang, F. Li, A. Cui, J. Hong, *Int. J. Hydrog. Energy*, 2018, **43,** 271-282.

30 A. Awadallah-F, S. A. Al-Muhtaseb, *Adsorption*, 2017, **23,** 933-944.

31 A. Awadallah-F, S. A. Al-Muhtaseb, *Adsorption*, 2013, **19**, 967-977.